A novel chlorophyll protein complex in the repair cycle of photosystem II

Daniel A. Weisz[a,1], Virginia M. Johnson[a,1], Dariusz M. Niedzwiedzki[b], Min Kyung Shinn[c,d], Haijun Liu[a], Clécio F. Klitzke[e,2], Michael L. Gross[e], Robert E. Blankenship[a], Timothy M. Lohman[c], and Himadri B. Pakrasi[a,3]

[a]Department of Biology, Washington University in St. Louis, St. Louis, MO 63130; [b]Center for Solar Energy & Energy Storage, Department of Energy, Environmental, & Chemical Engineering, Washington University in St. Louis, St. Louis, MO 63130; [c]Department of Biochemistry and Molecular Biophysics, Washington University School of Medicine, St. Louis, MO 63110; [d]Department of Physics, Washington University in St. Louis, St. Louis, MO 63130; and [e]Department of Chemistry, Washington University in St. Louis, St. Louis, MO 63130

Edited by Krishna K. Niyogi, University of California, Berkeley, CA, and approved September 19, 2019 (received for review June 4, 2019)

In oxygenic photosynthetic organisms, photosystem II (PSII) is a unique membrane protein complex that catalyzes light-driven oxidation of water. PSII undergoes frequent damage due to its demanding photochemistry. It must undergo a repair and reassembly process following photodamage, many facets of which remain unknown. We have discovered a PSII subcomplex that lacks 5 key PSII core reaction center polypeptides: D1, D2, PsbE, PsbF, and PsbI. This pigment–protein complex does contain the PSII core antenna proteins CP47 and CP43, as well as most of their associated low molecular mass subunits, and the assembly factor Psb27. Immunoblotting, mass spectrometry, and ultrafast spectroscopic results support the absence of a functional reaction center in this complex, which we call the "no reaction center" complex (NRC). Analytical ultracentrifugation and clear native PAGE analysis show that NRC is a stable pigment–protein complex and not a mixture of free CP47 and CP43 proteins. NRC appears in higher abundance in cells exposed to high light and impaired protein synthesis, and genetic deletion of PsbO on the PSII luminal side results in an increased NRC population, indicative that NRC forms in response to photodamage as part of the PSII repair process. Our finding challenges the current model of the PSII repair cycle and implies an alternative PSII repair strategy. Formation of this complex may maximize PSII repair economy by preserving intact PSII core antennas in a single complex available for PSII reassembly, minimizing the risk of randomly diluting multiple recycling components in the thylakoid membrane following a photodamage event.

photosynthesis | repair cycle | protein turnover | mass spectrometry | ultrafast spectroscopy

Photosystem II (PSII) is a large pigment–protein complex embedded in the thylakoid membrane of all oxygenic photosynthetic organisms: Cyanobacteria, algae, and plants. PSII plays a central role in energy flow in the biosphere by harnessing sunlight to split water molecules into protons, electrons, and molecular oxygen, ultimately yielding the vital high-energy molecules ATP and NADPH. This conversion of solar energy to chemical energy powers nearly all life on Earth, while simultaneously producing the oxygen we breathe.

Crystal structures of functional PSII (1–6) have revealed that the water-splitting reaction is catalyzed by a Mn_4CaO_5 (Mn) cluster bound to the luminal surface of PSII. D1 and D2, 2 ∼30-kDa transmembrane proteins, form a heterodimer at the center of PSII. They coordinate the primary electron transport chain cofactors and contribute most of the Mn-cluster ligands. D1 and D2 associate with the smaller (<10 kDa) subunits PsbE and PsbF (α- and β-subunits of cytochrome b_{559}) and PsbI. Together, these 5 proteins comprise the core "reaction center" (RC) complex, the smallest PSII subcomplex capable of light-induced charge separation (7). Surrounding the RC subunits are CP47 and CP43, 2 ∼50-kDa proteins that bind chlorophyll *a* (Chl *a*) molecules and serve as antennas, harvesting and funneling light energy toward the RC to drive PSII photochemistry. Around 10 additional low molecular mass (LMM) subunits bind to fully assembled PSII, contributing to the structural and functional optimization of the complex (8). Finally, functional PSII contains several membrane-extrinsic hydrophilic proteins (PsbO, PsbU, PsbV, and PsbQ in cyanobacteria) (9, 10), bound at the luminal surface of the complex, that stabilize the Mn cluster.

PSII undergoes frequent oxidative damage because of the demanding electron-transfer chemistry it performs (11–13). D1, closely followed by D2, is damaged and replaced most frequently of all proteins in the complex (14–18). However, CP47 and CP43 are more long lived (15, 17). This damage leads to partial disassembly of PSII, replacement of each damaged subunit with a new copy, and reassembly of PSII, in an intricate process known as the PSII repair cycle (14, 19, 20) (*SI Appendix*, Fig. S1). This cycle operates concurrently with de novo PSII synthesis. Synthesis of PSII occurs through stepwise assembly of PSII from component subcomplexes, in which the RC complex is joined with the CP47 precomplex first, followed by addition of the CP43 precomplex, and finally addition of membrane-extrinsic proteins (*SI Appendix*, Fig. S1). Current understanding is that repair occurs in much the same fashion, with removal of the extrinsic subunits, followed by the CP43 precomplex, replacement of D1 and/or D2 at the RC47

Significance

Photosystem II (PSII) converts sunlight into chemical energy, powering nearly all life on Earth. The efficiency of this process is maximized under various environmental conditions by a frequent repair and reassembly cycle that follows inevitable PSII damage even during normal oxygenic photosynthesis. We have isolated a pigment–protein PSII subcomplex in which, surprisingly, the reaction center (RC) components of PSII are absent. Formation of this stable chlorophyll–protein complex suggests a protective mechanism whereby longer-lived PSII subunits are "unplugged" from the damaged RC to prevent harmful, aberrant photochemistry during RC repair. This finding provides intriguing insight into how PSII is assembled and rebuilt to optimize its performance to optimally catalyze one of the most challenging reactions in biology.

Author contributions: D.A.W., V.M.J., M.L.G., R.E.B., T.M.L., and H.B.P. designed research; D.A.W., V.M.J., D.M.N., M.K.S., H.L., and C.F.K. performed research; D.A.W., V.M.J., D.M.N., M.K.S., H.L., and H.B.P. analyzed data; and D.A.W., V.M.J., D.M.N., M.K.S., H.L., M.L.G., R.E.B., T.M.L., and H.B.P. wrote the paper.

The authors declare no competing interest.

This article is a PNAS Direct Submission.

Data deposition: The mass spectrometry proteomics data have been deposited to the ProteomeXchange Consortium via the PRIDE partner repository (dataset identifier PXD013406).

[1]D.A.W. and V.M.J. contributed equally to this work.

[2]Present address: GCTOF Analytical Solution, Balneario Camboriu SC 88330-030 Brazil.

[3]To whom correspondence may be addressed. Email: Pakrasi@wustl.edu.

This article contains supporting information online at www.pnas.org/lookup/suppl/doi:10.1073/pnas.1909644116/-/DCSupplemental.

First published October 8, 2019.

level, and reassembly of PSII (14, 19, 20) (*SI Appendix*, Fig. S1). Many accessory proteins, such as Psb27 and Psb28 (21–25), bind exclusively to particular PSII subcomplexes to aid in a specific aspect of assembly. Despite this working model, our understanding is still evolving. Subcomplexes are low in abundance and transient in nature, and a complete characterization of all is far from complete. The steps that occur following photodamage are particularly uncertain, as repair subcomplexes are typically less amenable to targeted accumulation using PSII mutant strains than are intermediates of de novo assembly.

In this study, we describe the identification of a PSII subcomplex from the cyanobacterium *Synechocystis* sp. PCC 6803 (*Synechocystis* 6803). This subcomplex specifically lacks the 5 RC subunits, and therefore, we refer to it as the "no-RC" (NRC) complex. It accumulates to higher abundance in conditions of elevated PSII damage and impaired protein synthesis, leading us to conclude that the NRC is an intermediate in the repair cycle of PSII. A revised model of the repair steps following PSII photodamage is presented in light of our findings. We propose that NRC formation maximizes the efficiency of PSII repair and minimizes collateral damage to components of PSII that were unharmed following an initial photodamage event.

Results

Isolation of a PSII Subcomplex. We purified PSII complexes from the His47 and Δ*psb*O-His47 strains of *Synechocystis* 6803 by FPLC using a nickel-affinity column. His47 has a 6xHis-tag on the CP47 subunit of PSII, and Δ*psb*O-His47 is the same strain with an insertional deletion of the *psbO* gene. These complexes were then analyzed by high-resolution clear native acrylamide gel electrophoresis (Fig. 1*A*). As expected, in the Δ*psb*O-His47 strain, a major band was seen that represents the PSII monomer (PSII-M), whereas no PSII dimer was found as it is not formed in this strain (10, 25). Additionally, a green band just below the monomer was observed that corresponds to the RC47 complex previously observed in the literature (14, 20). In the His47 strain, a major band was seen that represents the PSII dimer (PSII-D), while PSII-M and the RC47 bands were also present. Interestingly, an additional green band of unknown identity was present at a lower molecular weight (MW) than the monomer in each strain. In-gel digestion followed by tandem mass spectrometry (MS) indicated sharply decreased D1, D2, and PsbE content in the lower MW band from both strains compared to PSII-M (Dataset S1), and presence of CP47 and CP43, although other assay methods were needed (see below) for more reliable quantitative information.

To obtain a sufficient quantity for further characterization of the unknown complex, PSII preparations were then subjected to glycerol gradient ultracentrifugation to separate distinct His-CP47–containing complexes (Fig. 1*B*). Again as expected, in the Δ*psb*O-His47 strain, a major band was seen that represents the PSII monomer (PSII-M), whereas no PSII dimer was found as it is not formed in this strain (10, 25), and in the His47 strain, a major band was seen that represents the PSII dimer (PSII-D) in addition to the monomer band. Consistent with the results in the clear native gel, a lower MW chlorophyll-containing band was observed in each strain. This band was harvested and concentrated. When the purified lower MW band from the *ΔpsbO* strain was run next to *ΔpsbO*-PSII by clear native gel electrophoresis, it comigrated with the band observed initially (*SI Appendix*, Fig. S2). Tandem MS was performed after in-solution digestion of the complex from Δ*psbO* cells. The dominant PSII proteins were CP47 and CP43. According to the semiquantitative information derived from such an experiment, levels of D1, D2, PsbE, and PsbF were markedly decreased compared to the corresponding PSII-M (Datasets S2 and S3), consistent with the results from in-gel digestion on the lower MW band described above.

The 77-K absorption spectra of *ΔpsbO*-PSII-M and the complex were nearly identical (Fig. 1*C*), with the exception that a small peak around 540 nm corresponding to pheophytin *a* (26) was absent in the spectrum of the complex. Pheophytin *a* is a cofactor in the PSII electron-transfer chain and is coordinated by D1 and D2.

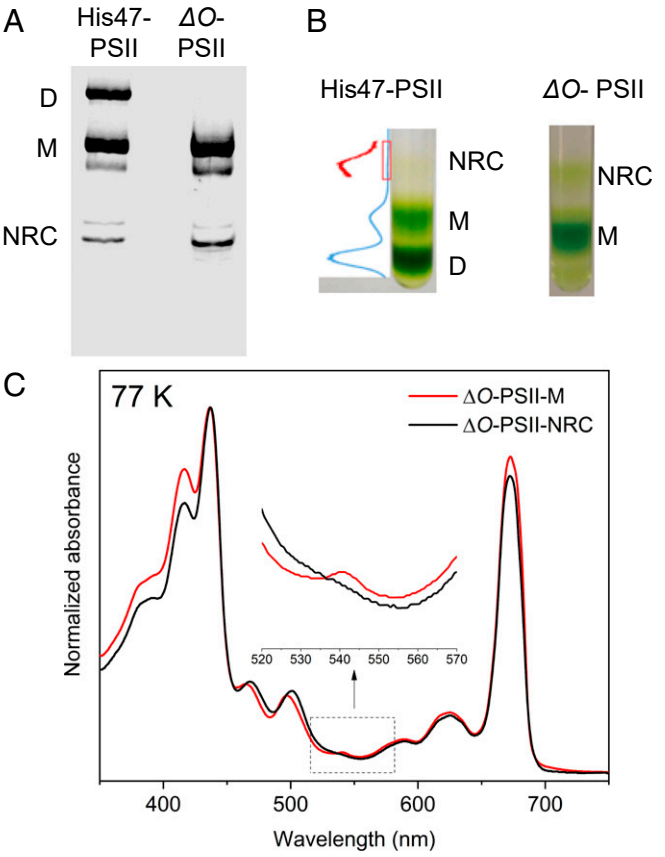

Fig. 1. Isolation and characterization of a PSII subcomplex (NRC). (*A*) Clear native PAGE of His-CP47–tagged PSII complexes from the His47 and Δ*psbO*-His47 strains. D, PSII dimer; M, PSII monomer. (*B*) Green bands corresponding to the NRC complex and PSII monomer (M) formed following ultracentrifugation of His-CP47–tagged PSII samples in a 5 to 30% linear glycerol gradient from the His47 and Δ*psbO*-His47 strains. Pixel intensity [plotted as inverse of gray value computed in ImageJ (55)] is shown on the left of the His47 gradient. The red curve shows the zoomed-in view of the region corresponding to the NRC band. (*C*) Steady-state absorption spectra of PSII-M and PSII-NRC at 77 K. To enable comparison, spectra were normalized to unity at the maximum of the Soret band (417 nm). The arrow shows a small peak visible in the spectrum of PSII-M that corresponds to the Q_x band of pheophytin *a* present in the PSII reaction center, and which is missing in the NRC spectrum.

SDS/PAGE analysis showed no band detectable for the core RC proteins D1 and D2 (Fig. 2*A*). However, it contained the inner antenna subunits CP47 and CP43, as well as Psb27, which binds to CP43 transiently during PSII assembly and repair (21, 22, 27, 28). In functional PSII, Chls *a* bound to CP47 and CP43 harvest light and transfer excitation energy to Chls *a* on D1 and D2, where primary PSII photochemistry occurs. A subcomplex containing both antenna proteins but lacking the 2 RC subunits to which they transfer energy was a surprising finding, as such a complex has not been observed previously and does not appear in the current model of the PSII lifecycle (*SI Appendix*, Fig. S1).

Consistent with SDS/PAGE, immunoblotting analysis (Fig. 2 *B* and *C*) showed no detectable levels of D1 and D2 in the complex isolated from both the *ΔpsbO* and His47 strains. Additionally, PsbE, another member of the PSII RC complex, was also absent (7). Presence of CP43 and CP47 in this complex, however, was confirmed, and the CP47-associated LMM subunit PsbH was detected as well. The MS results that showed severely decreased, but detectable, levels of D1 and D2 in the sample reflect the high sensitivity of the Q-Exactive MS instrument and the inevitability of some impurities remaining in the sample following purification. However, the SDS/PAGE and immunoblot results show that even

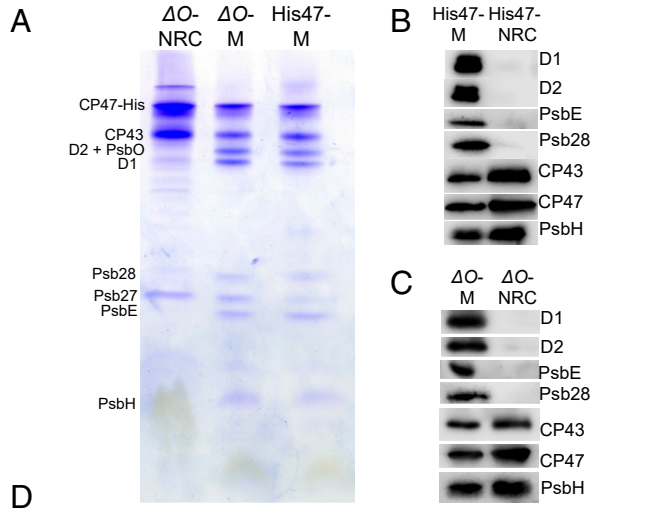

D

Protein	PSII Monomer	NRC	Observed mass (Da)	Calculated mass (Da)	Mass accu. (ppm)	Mod.	Example MS/MS ions observed (m/z)
PsbT	✓	✓	3565.93	3565.94	1	Form.	y_{24}^{2+}: 1373.29, y_{20}^{2+}: 1160.15
PsbM	✓	✓	3907.15	3907.15	<1	Form.	–
PsbK	✓	✓	4174.34	4174.33	2	-8 N Ter.	b_{16}^{+}: 1205.62, b_{24}^{+}: 1842.00
PsbX	✓	✓	4211.39	4211.37	4	Form.	y_{16}^{2+}: 987.57, y_{11}^{+}: 1322.74
PsbY	✓	✓	4227.35	4227.34	3	Form.	y_{21}^{2+}: 1075.60, y_{26}^{2+}: 1346.75
PsbI	✓	—	4331.35	4331.34	3	Form.	y_{22}^{2+}: 1265.64, y_{26}^{2+}: 1480.77
PsbL	✓	✓	4470.35	4470.35	<1	None	b_{27}^{3+}: 1022.55, b_{30}^{3+}: 1112.28
PsbF	✓	—	4798.56	4798.56	1	-M1	y_{11}^{+}: 1205.64, y_{14}^{+}: 1598.85
PsbH	✓	✓	6980.75	6980.75	<1	-M1	b_{33}^{3+}: 1150.62, b_{22}^{2+}: 1184.17
PsbE	✓	—	9311.65	9311.64	1	-M1	b_{26}^{3+}: 935.48, b_{34}^{3+}: 1278.34

Fig. 2. Major protein components of NRC. (*A*) SDS/PAGE analysis of PSII-M and PSII-NRC samples from the Δ*psbO*-His47 strain, and of PSII-M purified identically from the His47 strain. (*B*) Immunoblot analysis of PSII-M and PSII-NRC samples from the His47 strain. (*C*) Immunoblot analysis of PSII-M and PSII-NRC samples from the Δ*psbO*-His47 strain. (*D*) Summary table of the low-molecular mass subunits in Δ*O*-NRC detected by intact MS, including example fragment ions.

if small amounts of D1 and D2 are present below their detection limits, they are not stoichiometric components of this complex.

For a more complete identification of the LMM subunits in this complex, we employed MS to measure the mass of the intact protein components. We detected 10 LMM subunits in the control Δ*psbO*-PSII-M sample, whereas only 7 of those 10 were present in the identified complex (Fig. 2*D*, *SI Appendix*, Figs. S3 and S4, and Datasets S4 and S5). Remarkably, the 3 missing subunits are the 3 LMM components of the PSII RC: PsbE, PsbF, and PsbI. Taking our SDS/PAGE, immunoblot, and MS results together, we conclude that the subcomplex specifically lacks all 5 of the PSII RC components—D1, D2, PsbE, PsbF, and PsbI—but contains the rest of the PSII subunits observed in the control PSII-M sample. We therefore refer to it as the "no-reaction center" complex. The presence of the NRC in the His47 strain, seen through native gel, glycerol gradient, MS, and immunoblot characterization, demonstrates that this complex does not form as a result of the absence of PsbO in the Δ*psb*O-His47 strain. Unless otherwise mentioned, the experiments described below were, therefore, performed using the NRC from Δ*psb*O-His47 cells because of the higher yield obtainable in this strain.

Determination of the Size of the NRC Complex. The SDS/PAGE, Western blot, and MS results presented above identified the individual proteins in a denatured NRC sample. To determine the absolute MW of the intact, native complex, we used analytical ultracentrifugation (AUC). Distributions of the Chl-containing species of the PSII-M and NRC samples were determined from sedimentation velocity experiments using AUC (Fig. 3*A*). The NRC sample showed a major species at 6.1 S (Svedberg coefficient) (Fig. 3*A*, peak b), the molecular mass of which was determined as 167.0 ± 5.3 kDa in a subsequent sedimentation equilibrium experiment (Fig. 3*B*). A minor species at 2.9 S was also observed (Fig. 3*A*), with a molecular mass of 75.0 ± 3.5 kDa (Fig. 3*B*), which likely corresponds to dissociated CP47 (76 kDa) or CP43 (67 kDa) with their associated cofactors. For MW determination, the sedimentation equilibrium curves were analyzed using a 2-species fit based on the observation of 2 species from the sedimentation velocity experiments. The PSII-M sample showed a major species at 11.6 S (Fig. 3*A*, peak f), and 3 minor species at 2.9 S, 5.4 S, and 9.0 S. The molecular mass of the major species was estimated as 436 kDa, with a best-fit frictional coefficient ratio of 1.27, comparable to the MW of the PSII monomer determined in a previous study by Zouni et al. (29), using a similar method. The 3 minor species likely represent dissociation products.

The NRC Complex Lacks a Functional RC. The absence of the RC proteins in the NRC suggests that the complex cannot function as an RC. To test this hypothesis, we used ultrafast time-resolved fluorescence (TRF) measurements on the PSII-M and NRC samples. Both samples were excited at 625 nm, corresponding to a vibronic overtone of the Chl *a* Q_y band, and the Chl *a* fluorescence decay was monitored (Fig. 4 *A* and *B*, shown as pseudocolor 2D profiles). The profiles revealed substantial differences between the 2 samples. The initial fluorescence profile of PSII-M, with a fluorescence maximum at ∼680 nm, quickly evolved to a broader spectrum associated with another species with emission maximum at ∼700 nm, consistent with energy transfer from antennae to a trap (the RC). Fluorescence spectra profiles of Chl *a* in the NRC, however, remained relatively constant over time.

The differences were further emphasized through kinetic analysis of the TRF data (Fig. 4 *C* and *D*). Global analysis of the PSII-M and NRC spectra revealed 2 spectro-kinetic components (evolution associated fluorescence spectra) for each sample (see *Materials and Methods* for more details). The faster PSII-M and NRC components, with lifetimes of 250 and 330 ps, respectively, resemble each other and correspond to excitation equilibration within the protein. The slower PSII-M component, with a lifetime of 1.6 ns, was red-shifted and reflects excitation-energy transfer from CP47 and CP43 to deep energetic traps in the RC. These PSII-M results closely mimic those obtained for PSII core complexes from the cyanobacterium *Thermosynechococcus vulcanus* under similar conditions (30). The slower NRC component, however, with a lifetime of 4.6 ns, was very similar to the fast NRC component, suggesting that both originate from the same species. The lifetime of 4.6 ns closely resembled that obtained for isolated CP47 and CP43 proteins (31), implying that no further excitation energy transfer occurs in the NRC complex, and this component corresponds to intrinsic decay of excited Chl *a*. Overall, these results demonstrated that excitation energy in PSII-M that was initially localized on Chl *a* bound to CP47 and CP43, was efficiently transferred to the RC. In contrast, no such RC energy trap exists in the NRC complex, and excitation energy remained localized on CP47 and CP43 until it decayed intrinsically.

NRC Accumulates under High-Light Stress and in the Absence of Protein Synthesis. As the NRC is a previously unobserved subcomplex of PSII, we wished to determine whether NRC forms during de novo synthesis of PSII or during its repair cycle (*SI Appendix*, Fig. S1). This can be accomplished by observing whether NRC accumulates or is depleted under PSII-damaging conditions and following the addition of a protein synthesis inhibitor. Accumulation under such conditions indicates NRC formation during the repair cycle, while depletion indicates formation during de novo synthesis. To this end, His47 cultures were treated with either high light (HL, 400 μM photons/m^2·s), low light (LL, 40 μM photons/m^2·s, normal growth conditions), or these conditions with the addition of 20 μg lincomycin (HL+, LL+) to halt protein synthesis. Cells were harvested when the HL+ culture declined to 50% of the initial photosynthetic efficiency following a move to

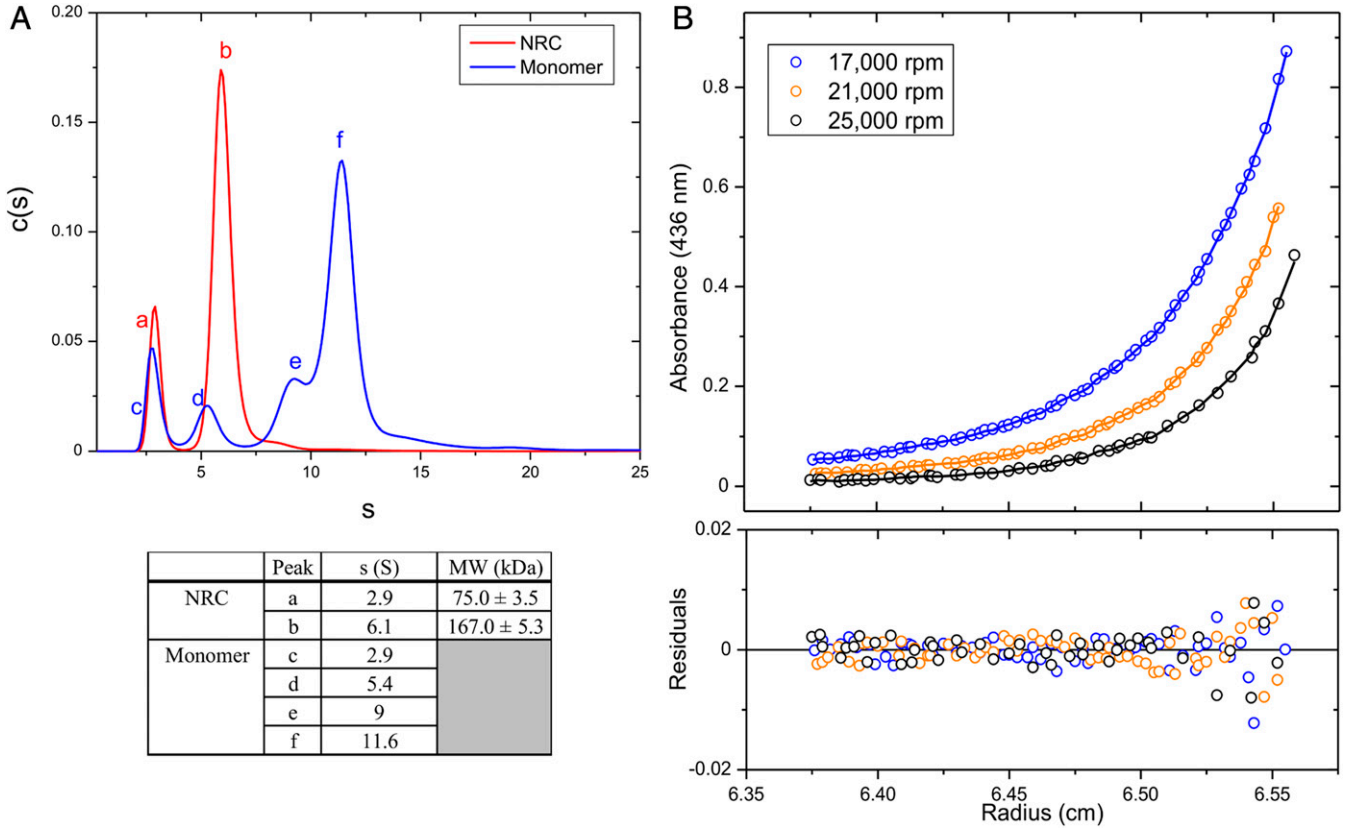

	Peak	s (S)	MW (kDa)
NRC	a	2.9	75.0 ± 3.5
	b	6.1	167.0 ± 5.3
Monomer	c	2.9	
	d	5.4	
	e	9	
	f	11.6	

Fig. 3. AUC to determine size of NRC and PSII-M (*A*) Relative distribution of components in Δ*O*-PSII-NRC (red) and Δ*O*-PSII-M (blue) samples based on Svedberg coefficient (S), and (*B*) MW determination of the NRC complex from sedimentation equilibrium analysis. For experimental and calculation details, see *Materials and Methods*.

HL and addition of lincomycin (F_v/F_m) (*SI Appendix*, Table S1). PSII was isolated from cultures grown under each of these conditions and PSII samples containing 10 μg Chl *a* were run on a clear native PAGE gel (Fig. 5*A* and *SI Appendix*, Fig. S5, for actual-color gel scan) to observe differences in NRC abundance. Intensities of each band were analyzed using the LI-COR analysis tool, and the ratios of the NRC/PSII monomer and NRC/PSII dimer were calculated for each condition (Fig. 5*B*). As seen in Fig. 5*A*, the HL+-treated cells have the highest quantity of NRC, and ratios of the NRC/PSII monomer and NRC/PSII dimer that are on average 10 times higher than the LL condition. LL+-treated cells follow in highest NRC abundance, with NRC/monomer and dimer ratios close to 3 times higher than the control LL condition. The HL-treated cells have a higher abundance of NRC (NRC/monomer and dimer ratios close to twice as high) than the LL control treatment, but the response is modest compared to those cells with impaired protein synthesis.

Discussion

In this study, we discovered and characterized the NRC complex, a PSII subcomplex that contains the inner antenna subunits CP43 and CP47, Psb27, and 7 LMM subunits, but is missing the 5 subunits that comprise the PSII RC: D1, D2, PsbE, PsbF, and PsbI. An assembled complex without all 5 RC components has not been described before. Through analytical sedimentation experiments, we determined the molecular mass of the NRC complex to be 167.0 ± 5.3 kDa. This value is in between the sum of the apo- (153 kDa) and holo- (194 kDa) masses of the NRC proteins, indicating that some NRC cofactors with D1 or D2 interfaces may be destabilized in their absence. The determined molecular mass is also close to the sum of the apparent masses of the individual CP43 and CP47 precomplexes (around 180 kDa) measured previously (32). These results are not consistent with the NRC sample comprising a mixture of separate CP43 and CP47 precomplexes, as each of these precomplexes have MWs roughly half of the determined MW. NRC is also not a mixture of homodimers of the CP43 and CP47 precomplexes. Given the respective sizes of the 2 precomplexes (32), such dimers would differ in mass by around 40 kDa, not consistent with the observed single, narrow, symmetrical major peak (Fig. 3, peak b), indicating a single species. Homodimers were also not detected during previous characterization of the precomplexes (32). Overall, the analytical sedimentation results indicate that the NRC complex is a single species likely composed of a single copy of each of the PSII subunits identified within.

The LMM subunits identified in NRC are consistent with the PSII crystal structures (2, 4, 5) in that all share interfaces with either CP43 or CP47 (except PsbY, which interfaces with another NRC subunit, PsbX). PsbH, PsbL, and PsbT were previously identified in the CP47 precomplex, and PsbK in the CP43 precomplex (32), consistent with our results. The presence of Psb27 is reasonable because it binds to CP43 (21, 28, 33), and the absence of Psb28 (Fig. 2 *B* and *C*) is also reasonable as Psb28 associates closely with PsbE and PsbF (25) and would not be expected to bind in their absence.

In the crystal structures of mature PSII, D1 and D2 bridge the gap in the transmembrane region between CP43 and CP47. In their absence, the NRC subunits do not form a continuous structure, except for a very small overlap between PsbL and PsbT at the cytosolic surface. A significant CP43–CP47 interface would likely be necessary to preserve the structural integrity of this complex and could occur with CP43 and CP47 approaching each other and at least partially closing the gap left by D1 and D2.

To test whether NRC occurs as an intermediate in the PSII repair cycle or as an intermediate in de novo PSII synthesis, we exposed His47 cells to HL to induce PSII damage and to lincomycin to stop protein synthesis, both separately and in

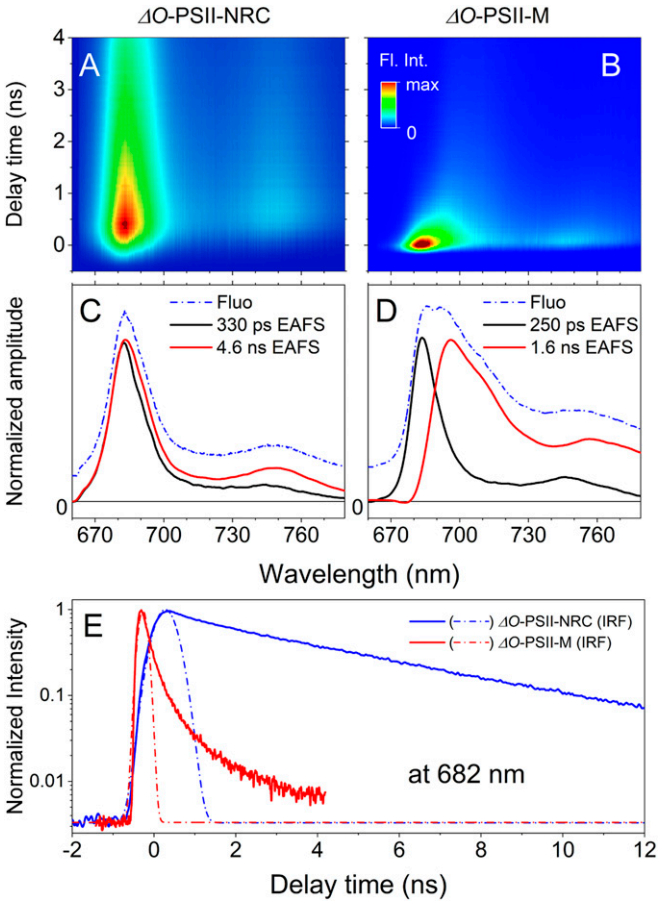

Fig. 4. TRF of ΔO-PSII-NRC and ΔO-PSII-M samples. (*A* and *B*) Two-dimensional pseudocolor fluorescence decay profiles at 77 K upon excitation at 625 nm. (*C* and *D*) Global analysis results of TRF datasets. Dashed profiles (Fluo) correspond to time-integrated spectra and mimic steady-state fluorescence spectra. All profiles were normalized at their maxima for better comparability. (*E*) Exemplary kinetic traces at 682 nm (maximum of fluorescence emission from CP47/CP43) accompanied with instrument response functions (IRF). Substantial shortening of fluorescence decay of the ΔO-PSII-M sample is associated with rapid excitation energy transfer from antenna into the PSII core (excitation trapping by reaction center). The different signal rise observed in the 2 traces originates from different temporal resolutions of time windows in which data were collected as demonstrated by IRF. EAFS, evolution associated fluorescence spectra.

combination with each other. If the NRC were an intermediate in the PSII repair cycle, formed as a result of damage to intact PSII, we expect that it would accumulate in HL, which causes increased PSII damage, and in the absence of protein synthesis, which would otherwise deplete existing NRC as D1 and D2 are resynthesized and inserted into the complex. Conversely, if the NRC were an intermediate in de novo PSII synthesis, we expect that NRC levels would remain stagnant or decrease in the absence of protein synthesis, as combination with newly synthesized D1 and D2 could not take place. Our results showed that the NRC increased in abundance by 2.2- and 2.7-fold compared to the PSII monomer and dimer, respectively, when His47 cultures were put into HL conditions damaging to PSII. A similar increase of 2.8- and 2.9-fold compared to monomer and dimer, respectively, was observed upon addition of lincomycin to stop protein synthesis under control LL conditions. The largest NRC increase, of 8.1- and 10.9-fold compared to monomer and dimer, respectively, occurred when cells were exposed to both HL and the presence of lincomycin (Fig. 5). These results are consistent with a model of the PSII lifecycle in which the NRC is an intermediate subcomplex in PSII repair and is not consistent with its formation during de novo synthesis. Furthermore, as more NRC accumulates in the absence of protein synthesis than in HL alone, we conclude that the NRC subunits are reincorporated into repaired PSII when newly synthesized D1 and D2 become available, depleting the level of the NRC in the thylakoid and completing the PSII repair cycle (Fig. 6). Our observation that the NRC:dimer ratio increased slightly more than the NRC:monomer ratio in all 3 conditions is consistent with this model, as photodamaged PSII dimers dissociate into monomers early in the PSII repair cycle.

Assignment of the NRC to the repair cycle also helps explain why this complex has not previously been detected. Most studies of PSII subcomplexes have focused on the assembly of PSII, not the intermediates that form following photodamage. Many of these studies used mutants that block assembly before formation of active PSII (e.g., ΔCtpA, ΔD2, ΔCP43, or ΔCP47 strains). This valuable strategy has enabled isolation of numerous de novo assembly intermediates, but as active PSII is never formed in these strains, it has precluded the possibility of observing NRC (27, 28, 34, 35).

The currently known steps in the PSII repair process are: 1) Dissociation of the extrinsic proteins PsbO, PsbU, PsbV, and PsbQ (36); 2) rebinding of Psb27 (22); 3) monomerization of the complex (36); 4) an undefined further dissociation step (20); 5) D1 degradation (37–39); 6) insertion of a new D1 copy (14); and 7) PSII reassembly (14). Within this known framework, NRC formation would most logically occupy step 4, the undefined dissociation step, with the damaged Psb27-PSII monomer splitting into RC and NRC components (Fig. 6; note that steps 1 to 3 are omitted in Fig. 6 and *SI Appendix*, Fig. S1 for clarity). An implication is that D1 (and D2) replacement would occur at the level of the RC complex (Fig. 6), not at RC47 as has been previously proposed (*SI Appendix*, Fig. S1) (14, 20, 40). Meanwhile, the longer-lived (15) CP43 and CP47 would be sequestered efficiently in one location, ready to be recycled back into PSII after synthesis of a new D1 and D2 (15). Dissociation of PSII into RC and NRC complexes following photodamage would allow maximal access for proteases to both D1 and D2, whereas, by interacting closely, CP43 and CP47 would shield each other from such protease attack (41). The recent interesting finding that PSII can remain stable and fully intact following Mn cluster removal (42) supports the notion that there may be an important efficiency benefit to maintaining a PSII subcomplex, once assembled, in as intact a state as possible, while still allowing for necessary repair to occur.

Damaged PSII is a liability because aberrant PSII photochemistry could result in further oxidative damage to the complex. During PSII assembly, D1 processing is a checkpoint that prevents premature formation of the highly oxidizing Mn cluster, which could result in damage to nearby subunits (27). The dissociation of the extrinsic proteins and the rebinding of Psb27 following photodamage likely achieves the same goal: Inactivation of the Mn cluster at a time when it could only cause further damage. The formation of the NRC complex can be understood in a similar manner. In addition to being an efficient disassembly/reassembly mechanism, separating into RC and NRC complexes following initial damage to D1 or D2 could serve a 2-fold protective purpose:

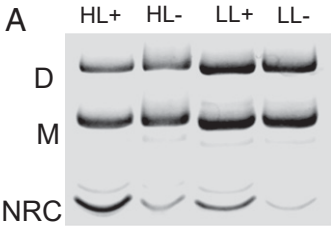

B

	NRC/M	NRC/D
HL+	0.81	1.20
HL-	0.22	0.30
LL+	0.28	0.32
LL-	0.10	0.11

Fig. 5. Clear native PAGE of HL treated PSII samples. (*A*) Clear native PAGE of His-CP47–tagged PSII complexes from cultures treated with HL, LL, and with or without (±) 20 μg/mL lincomycin. D, PSII dimer; M, PSII monomer. (*B*) Table of ratios of band intensities from *A* calculated using the LI-COR analysis tool.

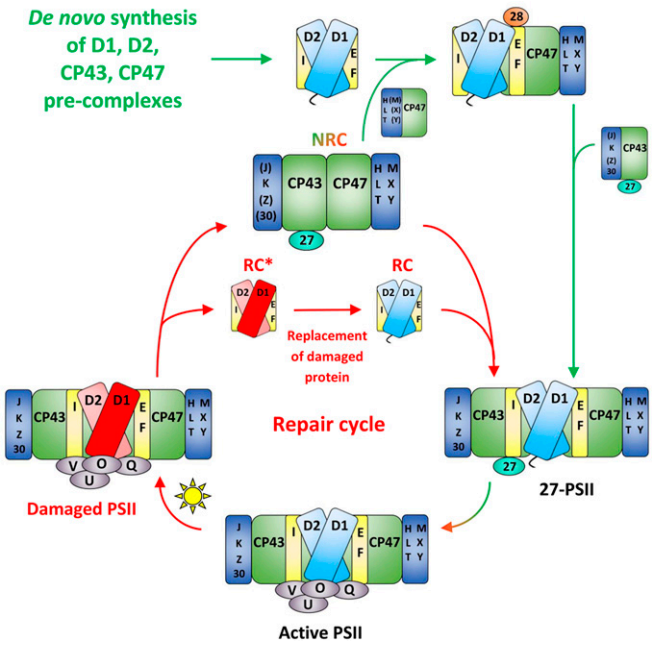

Fig. 6. Schematic of the PSII life cycle based on previous findings (reviewed in refs. 14, 19, 36, and 56) and current results, focusing on the proposed positioning of the NRC in the RC. Red arrows, repair cycle steps; red D1, damaged version of D1; light red D2, slightly less frequently damaged version of D2. In a given RC* complex, either D1, D2, or both may be damaged. Several intermediary stages (steps 1 to 3 in *Discussion*) in the life cycle are omitted for clarity: After damage, PsbO, PsbU, PsbV, and PsbQ dissociate (36), Psb27 rebinds (22), and the complex monomerizes (36) before the proposed NRC formation step. Black text and red/green coloring represent steps common to both de novo synthesis and repair.

1) It lowers the total excitation energy reaching the RC by "unplugging" it from the CP47 and CP43 antenna subunits, and 2) it prevents aberrant PSII photochemistry from causing collateral damage to the NRC components, which are unlikely to have been harmed in the initial photodamage event. Future structural studies of the NRC Chl–protein complex are expected to shed light on the dynamic process during the PSII repair cycle.

Materials and Methods

Cell Culture, PSII Purification, and Protein Analysis. Generation of the Δ*psb*O-His47 strain was reported previously (10). The HT3 (His47) strain was a kind gift from Terry Bricker, Louisiana State University, Baton Rouge, LA (43). Cyanobacterial strains were grown in BG11 medium at 30 °C under 40 μmol photons m^{-2} s^{-1}. The growth media were supplemented with 10 μg/mL spectinomycin and 5 μg/mL gentamicin (Δ*psb*O-His47 strain) or 5 μg/mL gentamicin (His47 strain). Histidine-tagged PSII complexes were purified by FPLC, as described previously (44), with minor modifications, and were stored in RB buffer: 25% glycerol (wt/vol), 10 mM $MgCl_2$, 5 mM $CaCl_2$, 50 mM MES buffer pH 6.0. Following FPLC purification, PSII complexes were purified further by glycerol gradient ultracentrifugation, performed as described previously (25). See *SI Appendix, SI Methods* for more detail. Protein electrophoresis was performed as described previously (45, 46). For immunoblotting, gels were transferred onto a PVDF membrane (Millipore Sigma) followed by probing with specific antisera. Immunoblot imaging was performed with chemiluminescence reagents (Millipore Sigma) on a LI-COR Odyssey Fc (LI-COR Biotechnology).

Clear Native PAGE. High-resolution clear native PAGE was performed as described in ref. 47. Protein samples containing 10 μg of Chl *a* were loaded in each lane. Gel was run at 4 mA for 16 h at 4 °C and imaged using a LI-COR Odyssey Fc (LI-COR Biotechnology) using the 700-nm channel.

In-Gel Digestion and LC-MS/MS Analysis. Protein samples were excised from the clear native polyacrylamide gel, destained, dehydrated, and digested in-gel with 13 ng/uL trypsin (Sigma) in 1 mM triethylammonium bicarbonate. Following digestion, sample was extracted in 1% formic acid and subjected to LC-MS/MS. For detailed MS methods and data analysis, see *SI Appendix, SI Methods*.

In-Solution Digestion and LC-MS/MS Analysis. Samples each containing 2 μg Chl *a* of Δ*psb*O-PSII-M and Δ*psb*O-NRC were precipitated using the 2D Cleanup Kit (GE Healthcare). The pellets were resuspended in 20 μL 8 M urea, 50 mM ammonium bicarbonate (ABC). Lys C was added at a 1:50 (wt/wt) protease:sample ratio and incubated at 37 °C for 2 h. Samples were diluted to 1 M urea with 50 mM ABC and trypsin was added at a 1:50 (wt/wt) protease: sample ratio. The samples were incubated overnight at 37 °C, then acidified to 1% formic acid and centrifuged to remove any insoluble material. Digests were analyzed by LC-MS/MS as described in ref. 25. For detailed methods, see *SI Appendix, SI Methods*. The mass spectrometry proteomics data have been deposited to the ProteomeXchange Consortium via the PRIDE (48) partner repository with the dataset identifier PXD013406 and 10.6019/PXD013406 (49).

MS of Intact Proteins. Δ*O*-M and Δ*O*-NRC samples, each containing 1.4 μg Chl *a*, were precipitated using the 2D Cleanup Kit (GE Healthcare). The pellets were resuspended in 100 μL 70% acetone, 19% water, 10% isopropanol, 1% formic acid (vol/vol) (32), diluted 1:3 in the resuspension solution, and infused directly into a Synapt G2 HDMS mass spectrometer (Waters). For detailed methods, see *SI Appendix, SI Methods*.

Ultrafast TRF Spectroscopy. All spectroscopic measurements were carried out at 77 K, using a VNF-100 liquid nitrogen cryostat (Janis). The samples were diluted in 60:40 (vol/vol) glycerol:RB buffer with 0.04% DM, that after cooling, formed fully transparent glass. Steady-state absorption spectra were recorded on a UV-1800 spectrophotometer (Shimadzu). TRF imaging was performed using a universal streak camera system (Hamamatsu) based on an N51716-04 streak tube and A6365-01 spectrograph from the Bruker Corporation coupled to an ultrafast laser system, described previously (50). For more detailed methods and data analysis, see *SI Appendix, SI Methods*,

Analytical Sedimentation. After sample concentration following glycerol gradient ultracentrifugation (see above), Δ*O*-M and Δ*O*-NRC samples were buffer-exchanged into RB buffer pH 6.5 containing 5% glycerol. Sedimentation velocity experiments were performed with an Optima XL-A analytical ultracentrifuge and An50Ti rotor (Beckman Instruments) at 42,000 rpm (25 °C), as described previously (51). The experiment was performed at 4 and 13 μg/mL Chl *a*, while monitoring absorbance at 437 nm, with the results consistent at both concentrations. Data were analyzed using SEDFIT (52), to obtain c(s) distributions. The c(s) distribution function defines the populations of species with different sedimentation rates (sizes) and represents a variant of the distribution of Lamm equation solutions (52). The density and viscosity of the RB buffer at 25 °C were determined using SEDNTERP; 0.76 mL/g was used as the partial specific volume (29).

Sedimentation equilibrium experiments were performed with the NRC sample at the 3 indicated speeds (25 °C) starting at the lowest and finishing at the highest speed, as described previously (53). Next, 110 μL of the NRC sample at the same concentration used for the sedimentation velocity experiments and 120 μL of the buffer was loaded to an Epon charcoal-filled 6-channel centerpiece. Absorbance data were collected at intervals of 0.003 cm in the step mode with 5 averages per step. Data were edited using SEDFIT to extract concentration profiles from each chamber and analyzed using SEDPHAT with the Species Analysis with Mass Conservation model (54).

PSII Damage Induction. His47 cells were grown to late log phase under conditions described above, and then divided and allowed to grow for 3 h before being subjected to either HL and lincomycin (400 μmol photons/m^2·s and 20 μg/mL lincomycin), HL without lincomycin, LL and lincomycin (40 μmol photons/m^2·s and 20 μg/mL lincomycin), or LL without lincomycin. After 5 h under these conditions, when photosynthetic efficiency decreased to 50% for the HL and lincomycin treatment, cells were harvested and PSII was isolated as described above. Photosynthetic efficiency (F_v/F_m) was monitored using an FL-200 fluorometer (PSI).

ACKNOWLEDGMENTS. We thank Dr. Alexander Kozlov for helpful discussions. This work was supported by the Chemical Sciences, Geosciences, and Biosciences Division, Office of Basic Energy Sciences, Office of Science, US Department of Energy (DOE) Grant DE-FG02-99ER20350 (to H.B.P.); the Photosynthetic Antenna Research Center, an Energy Frontier Research Center funded by the US DOE, Office of Basic Energy Sciences Grant DE-SC 0001035 (to H.B.P., R.E.B., and M.L.G.); NIH Grant P41GM103422 (to M.L.G.); and NIH Grant GM030498 (to T.M.L.). V.M.J. was supported by a training Grant T32 EB014855 from the National Institute of Biomedical Imaging and Bioengineering, NIH.

1. M. Suga *et al*., Native structure of photosystem II at 1.95 Å resolution viewed by femtosecond X-ray pulses. *Nature* **517**, 99–103 (2015).
2. M. Suga *et al*., Light-induced structural changes and the site of O=O bond formation in PSII caught by XFEL. *Nature* **543**, 131–135 (2017).
3. C. Kupitz *et al*., Serial time-resolved crystallography of photosystem II using a femtosecond X-ray laser. *Nature* **513**, 261–265 (2014).
4. Y. Umena, K. Kawakami, J. R. Shen, N. Kamiya, Crystal structure of oxygen-evolving photosystem II at a resolution of 1.9 Å. *Nature* **473**, 55–60 (2011).
5. A. Zouni *et al*., Crystal structure of photosystem II from Synechococcus elongatus at 3.8 A resolution. *Nature* **409**, 739–743 (2001).
6. I. D. Young *et al*., Structure of photosystem II and substrate binding at room temperature. *Nature* **540**, 453–457 (2016).
7. O. Nanba, K. Satoh, Isolation of a photosystem II reaction center consisting of D-1 and D-2 polypeptides and cytochrome *b*-559. *Proc. Natl. Acad. Sci. U.S.A.* **84**, 109–112 (1987).
8. L. X. Shi, M. Hall, C. Funk, W. P. Schröder, Photosystem II, a growing complex: Updates on newly discovered components and low molecular mass proteins. *Biochim. Biophys. Acta* **1817**, 13–25 (2012).
9. J. L. Roose, L. K. Frankel, M. P. Mummadisetti, T. M. Bricker, The extrinsic proteins of photosystem II: Update. *Planta* **243**, 889–908 (2016).
10. H. Liu *et al*., MS-based cross-linking analysis reveals the location of the PsbQ protein in cyanobacterial photosystem II. *Proc. Natl. Acad. Sci. U.S.A.* **111**, 4638–4643 (2014).
11. D. A. Weisz, M. L. Gross, H. B. Pakrasi, Reactive oxygen species leave a damage trail that reveals water channels in photosystem II. *Sci. Adv.* **3**, eaao3013 (2017).
12. R. Kale *et al*., Amino acid oxidation of the D1 and D2 proteins by oxygen radicals during photoinhibition of photosystem II. *Proc. Natl. Acad. Sci. U.S.A.* **114**, 2988–2993 (2017).
13. P. Pospíšil, Production of reactive oxygen species by photosystem II as a response to light and temperature stress. *Front. Plant Sci.* **7**, 1950 (2016).
14. J. Nickelsen, B. Rengstl, Photosystem II assembly: From cyanobacteria to plants. *Annu. Rev. Plant Biol.* **64**, 609–635 (2013).
15. D. C. Yao, D. C. Brune, W. F. Vermaas, Lifetimes of photosystem I and II proteins in the cyanobacterium *Synechocystis* sp. PCC 6803. *FEBS Lett.* **586**, 169–173 (2012).
16. J. Komenda, J. Masojídek, Functional and structural changes of the photosystem II complex induced by high irradiance in cyanobacterial cells. *Eur. J. Biochem.* **233**, 677–682 (1995).
17. D. A. Christopher, J. E. Mullet, Separate photosensory pathways co-regulate blue light/ultraviolet-A-activated *psb*D-*psb*C transcription and light-induced D2 and CP43 degradation in barley (*Hordeum vulgare*) chloroplasts. *Plant Physiol.* **104**, 1119–1129 (1994).
18. E. M. Bonisteel *et al*., Strain specific differences in rates of Photosystem II repair in picocyanobacteria correlate to differences in FtsH protein levels and isoform expression patterns. *PLoS One* **13**, e0209115 (2018).
19. D. A. Weisz, M. L. Gross, H. B. Pakrasi, The use of advanced mass spectrometry to dissect the life-cycle of photosystem II. *Front. Plant Sci.* **7**, 617 (2016).
20. J. Komenda, R. Sobotka, P. J. Nixon, Assembling and maintaining the photosystem II complex in chloroplasts and cyanobacteria. *Curr. Opin. Plant Biol.* **15**, 245–251 (2012).
21. H. Liu, R. Y. Huang, J. Chen, M. L. Gross, H. B. Pakrasi, Psb27, a transiently associated protein, binds to the chlorophyll binding protein CP43 in photosystem II assembly intermediates. *Proc. Natl. Acad. Sci. U.S.A.* **108**, 18536–18541 (2011).
22. N. Grasse *et al*., Role of novel dimeric Photosystem II (PSII)-Psb27 protein complex in PSII repair. *J. Biol. Chem.* **286**, 29548–29555 (2011).
23. J. L. Roose, H. B. Pakrasi, The Psb27 protein facilitates manganese cluster assembly in photosystem II. *J. Biol. Chem.* **283**, 4044–4050 (2008).
24. M. Dobáková, R. Sobotka, M. Tichý, J. Komenda, Psb28 protein is involved in the biogenesis of the photosystem II inner antenna CP47 (PsbB) in the cyanobacterium *Synechocystis* sp. PCC 6803. *Plant Physiol.* **149**, 1076–1086 (2009).
25. D. A. Weisz *et al*., Mass spectrometry-based cross-linking study shows that the Psb28 protein binds to cytochrome b_{559} in photosystem II. *Proc. Natl. Acad. Sci. U.S.A.* **114**, 2224–2229 (2017).
26. M. Rögner, D. A. Chisholm, B. A. Diner, Site-directed mutagenesis of the *psb*C gene of photosystem II: Isolation and functional characterization of CP43-less photosystem II core complexes. *Biochemistry* **30**, 5387–5395 (1991).
27. H. Liu, J. L. Roose, J. C. Cameron, H. B. Pakrasi, A genetically tagged Psb27 protein allows purification of two consecutive photosystem II (PSII) assembly intermediates in *Synechocystis* 6803, a cyanobacterium. *J. Biol. Chem.* **286**, 24865–24871 (2011).
28. J. Komenda *et al*., The Psb27 assembly factor binds to the CP43 complex of photosystem II in the cyanobacterium *Synechocystis* sp. PCC 6803. *Plant Physiol.* **158**, 476–486 (2012).
29. A. Zouni *et al*., Size determination of cyanobacterial and higher plant photosystem II by gel permeation chromatography, light scattering, and ultracentrifugation. *Biochemistry* **44**, 4572–4581 (2005).
30. Y. Shibata, S. Nishi, K. Kawakami, J. R. Shen, T. Renger, Photosystem II does not possess a simple excitation energy funnel: Time-resolved fluorescence spectroscopy meets theory. *J. Am. Chem. Soc.* **135**, 6903–6914 (2013).
31. A. P. Casazza, M. Szczepaniak, M. G. Müller, G. Zucchelli, A. R. Holzwarth, Energy transfer processes in the isolated core antenna complexes CP43 and CP47 of photosystem II. *Biochim. Biophys. Acta* **1797**, 1606–1616 (2010).
32. M. Boehm *et al*., Investigating the early stages of photosystem II assembly in *Synechocystis* sp. PCC 6803: Isolation of CP47 and CP43 complexes. *J. Biol. Chem.* **286**, 14812–14819 (2011).
33. K. U. Cormann, M. Möller, M. M. Nowaczyk, Critical assessment of protein cross-linking and molecular docking: An updated model for the interaction between photosystem II and Psb27. *Front. Plant Sci.* **7**, 157 (2016).
34. M. Boehm *et al*., Subunit composition of CP43-less photosystem II complexes of Synechocystis sp. PCC 6803: Implications for the assembly and repair of photosystem II. *Philos. Trans. R. Soc. Lond. B Biol. Sci.* **367**, 3444–3454 (2012).
35. J. Komenda *et al*., Accumulation of the D2 protein is a key regulatory step for assembly of the photosystem II reaction center complex in Synechocystis PCC 6803. *J. Biol. Chem.* **279**, 48620–48629 (2004).
36. P. D. Mabbitt, S. M. Wilbanks, J. J. Eaton-Rye, Structure and function of the hydrophilic photosystem II assembly proteins: Psb27, Psb28 and Ycf48. *Plant Physiol. Biochem.* **81**, 96–107 (2014).
37. J. Komenda *et al*., The FtsH protease slr0228 is important for quality control of photosystem II in the thylakoid membrane of *Synechocystis* sp. PCC 6803. *J. Biol. Chem.* **281**, 1145–1151 (2006).
38. J. Sacharz *et al*., Sub-cellular location of FtsH proteases in the cyanobacterium *Synechocystis* sp. PCC 6803 suggests localised PSII repair zones in the thylakoid membranes. *Mol. Microbiol.* **96**, 448–462 (2015).
39. M. Boehm *et al*., Subunit organization of a *synechocystis* hetero-oligomeric thylakoid FtsH complex involved in photosystem II repair. *Plant Cell* **24**, 3669–3683 (2012).
40. P. J. Nixon, M. Barker, M. Boehm, R. de Vries, J. Komenda, FtsH-mediated repair of the photosystem II complex in response to light stress. *J. Exp. Bot.* **56**, 357–363 (2005).
41. V. Krynická, S. Shao, P. J. Nixon, J. Komenda, Accessibility controls selective degradation of photosystem II subunits by FtsH protease. *Nat. Plants* **1**, 15168 (2015).
42. M. Zhang *et al*., Structural insights into the light-driven auto-assembly process of the water-oxidizing Mn_4CaO_5-cluster in photosystem II. *eLife* **6**, e26933 (2017).
43. T. M. Bricker, J. Morvant, N. Masri, H. M. Sutton, L. K. Frankel, Isolation of a highly active photosystem II preparation from *Synechocystis* 6803 using a histidine-tagged mutant of CP 47. *Biochim. Biophys. Acta* **1409**, 50–57 (1998).
44. Y. Kashino *et al*., Proteomic analysis of a highly active photosystem II preparation from the cyanobacterium *Synechocystis* sp. PCC 6803 reveals the presence of novel polypeptides. *Biochemistry* **41**, 8004–8012 (2002).
45. Y. Kashino, H. Koike, K. Satoh, An improved sodium dodecyl sulfate-polyacrylamide gel electrophoresis system for the analysis of membrane protein complexes. *Electrophoresis* **22**, 1004–1007 (2001).
46. Y. Kashino *et al*., Low-molecular-mass polypeptide components of a photosystem II preparation from the thermophilic cyanobacterium *Thermosynechococcus vulcanus*. *Plant Cell Physiol.* **43**, 1366–1373 (2002).
47. I. Wittig, M. Karas, H. Schägger, High resolution clear native electrophoresis for in-gel functional assays and fluorescence studies of membrane protein complexes. *Mol. Cell. Proteomics* **6**, 1215–1225 (2007).
48. Y. Perez-Riverol, *et al*., The PRIDE database and related tools and resources in 2019: Improving support for quantification data. *Nucleic Acids Res.* **47**, D442–D450 (2019).
49. H. Liu, Photosystem II assembly No-reaction center (NRC) complex. PRIDE repository. https://www.ebi.ac.uk/pride/archive/projects/PXD013406. Deposited 8 April 2019.
50. D. M. Niedzwiedzki, J. Jiang, C. S. Lo, R. E. Blankenship, Low-temperature spectroscopic properties of the peridinin-chlorophyll *a*-protein (PCP) complex from the coral symbiotic dinoflagellate *Symbiodinium*. *J. Phys. Chem. B* **117**, 11091–11099 (2013).
51. A. G. Kozlov, M. K. Shinn, E. A. Weiland, T. M. Lohman, Glutamate promotes SSB protein-protein Interactions via intrinsically disordered regions. *J. Mol. Biol.* **429**, 2790–2801 (2017).
52. J. Dam, P. Schuck, Calculating sedimentation coefficient distributions by direct modeling of sedimentation velocity concentration profiles. *Methods Enzymol.* **384**, 185–212 (2004).
53. A. Niedziela-Majka, N. K. Maluf, E. Antony, T. M. Lohman, Self-assembly of *Escherichia coli* MutL and its complexes with DNA. *Biochemistry* **50**, 7868–7880 (2011).
54. J. Vistica *et al*., Sedimentation equilibrium analysis of protein interactions with global implicit mass conservation constraints and systematic noise decomposition. *Anal. Biochem.* **326**, 234–256 (2004).
55. C. A. Schneider, W. S. Rasband, K. W. Eliceiri, NIH Image to ImageJ: 25 years of image analysis. *Nat. Methods* **9**, 671–675 (2012).
56. S. Heinz, P. Liauw, J. Nickelsen, M. Nowaczyk, Analysis of photosystem II biogenesis in cyanobacteria. *Biochim. Biophys. Acta* **1857**, 274–287 (2016).